Journal of Leather Science and Engineering

RESEARCH Open Access

Visible-light-driven photocatalytic degradation of rhodamine B using Bi_2WO_6/GO deposited on polyethylene terephthalate fabric

Zoufei Du[1], Ce Cui[2], Sihang Zhang[1], Hongyan Xiao[2], Erhui Ren[2], Ronghui Guo[2*] and Shouxiang Jiang[3*]

Abstract

The environmental repercussions of wastewater from the dye process mean that it is very important to obtain an eco-friendly photocatalyst that would degrade wastewater. Herein, bismuth tungstate/graphene oxide (Bi_2WO_6/GO) composites are fabricated through in-situ hydrothermal reaction and then the Bi_2WO_6/GO photocatalysts are deposited onto polyethylene terephthalate (PET) fabric. The obtained Bi_2WO_6/GO deposited PET fabrics are then characterized through XPS, Raman, SEM, TEM, XRD, UV-vis, BET method and photoluminescence spectroscopy (PL) to investigate their chemical and crystal structures, morphology, optical property, surface area and photochemical properties. Photocatalytic performance is studied through examining the rate of degrading rhodamine B (RhB) under visible light. Surface of PET fibers is densely covered with Bi_2WO_6/GO. Bi_2WO_6/GO deposited PET fabrics show a broad absorption band in the visible spectra. Removal rate of RhB on the Bi_2WO_6/GO deposited PET fabric is the highest with the GO content of 2 g/L (labeled as Bi_2WO_6/2 g/LGO). The result of active species experiment shows that superoxide radicals ($\cdot O_2^-$) plays a major role in the degradation of RhB. Moreover, Bi_2WO_6/2 g/LGO deposited PET fabric shows excellent cycle stability of photocatalytic degradation for RhB. The findings in this work can be extended to preparation other types of composite on the textile for photocatalysis, which can be applied to remove dyes in the wastewater produced by the textile or leather industry.

Keywords: Bi_2WO_6/GO depositing, RhB, PET fabric, Photocatalytic performance, Visible light-driven

1 Introduction

It is well known that industries can contribute to the contamination of water bodies, such as textile and leather industries because a large volume of water is used in the process, generating large amounts of effluents. The dye wastewater from these industries is resistant to biodegradation [1]. Therefore, industrial dye wastewater treatment has received much attention. Among numerous pollutant treatment approaches, photocatalysis is one of the most promising methods for wastewater treatment [2–4]. In recent years, Bi-based photocatalysts have attracted much attention [5–7]. Bi_2WO_6 is reported as an effective photocatalyst for detoxification in wastewater as well as polluted air among Bi-based semiconductors. Additionally, Bi_2WO_6 is stable with high activity because the octahedron of ceratoid WO_6 is situated in the sandwich of $(Bi_2O_2)^{2+}$ and can improve the separation of photo-generated charges [8, 9]. Nevertheless, the photocatalytic performance of pristine Bi_2WO_6 is restricted due to its low light absorption, difficult migration and rapid recombination of photo-generated electron-hole pairs [10, 11]. In this sense, various efficient methods and technologies have been reported such

* Correspondence: ronghuiguo214@126.com; kinor.j@polyu.edu.hk
[2]College of Biomass Science and Engineering, Sichuan University, No.24 South Section 1, Yihuan Road, Chengdu, China
[3]Institute of Textiles and Clothing, The Hong Kong Polytechnic University, Hung Hom, Kowloon, Hong Kong, China
Full list of author information is available at the end of the article

Springer Open

© The Author(s). 2020 **Open Access** This article is licensed under a Creative Commons Attribution 4.0 International License, which permits use, sharing, adaptation, distribution and reproduction in any medium or format, as long as you give appropriate credit to the original author(s) and the source, provide a link to the Creative Commons licence, and indicate if changes were made. The images or other third party material in this article are included in the article's Creative Commons licence, unless indicated otherwise in a credit line to the material. If material is not included in the article's Creative Commons licence and your intended use is not permitted by statutory regulation or exceeds the permitted use, you will need to obtain permission directly from the copyright holder. To view a copy of this licence, visit http://creativecommons.org/licenses/by/4.0/.

as doping, substitution, heterostructure building with a narrow-bandgap semiconductor and coupling with a carrier to increase the photoinduced electron-hole pair's separation and transfer of Bi_2WO_6 [12–14].

Graphene oxide (GO) contains functional groups like hydroxyl and epoxide groups on the basal plane and carboxyl groups at the edge [15]. The presence of π-conjugation systems and oxygen groups cause GO to absorb visible light and impart high hydrophilicity to GO. In addition, GO can be readily dispersed in water at the molecular level, which exhibits biocompatibility and possesses tunable band gap. These can inspire this study to explore its potential as a photocatalytic material [16, 17]. To date, there have been some reports on the fabrication of bismuth tungstate/graphene oxide (Bi_2WO_6/GO) for photocatalytic degradation of organic dyes [18, 19].

Up to date, most researchers mainly focus on the study of the photocatalytic property of Bi_2WO_6/GO powders. However, it is not easy for the Bi_2WO_6/GO powder to be separated and recycled from the dye solution during the photocatalysis. In order to overcome these difficulties, some photocatalysts have deposited on textile products to investigate the photocatalytic activity of deposited fabrics in our previous reports such as Bi_2WO_6 and Bi_2WO_6/TiO_2 [20, 21]. Up to now, there are no reports about Bi_2WO_6/GO composite photocatalysts depositing on textiles for the dye degradation.

In this work, Bi_2WO_6 and GO was complexed and treated by a facile hydrothermal method to obtain Bi_2WO_6/GO and they were then deposited on the PET fabric. The structure, photo-adsorption characteristics and specific surface area of the as- Bi_2WO_6/GO deposited PET fabrics were studied by SEM, TEM, XPS, Raman, XRD, UV-vis, PL and BET. The photocatalytic performance and recyclability of the Bi_2WO_6/GO deposited PET fabrics were investigated by the decomposition of RhB under visible light. Besides, effect of GO concentration on the photocatalytic properties of Bi_2WO_6/GO deposited PET fabric was studied.

2 Experimental

2.1 Materials

PET fabrics were selected as the substrate. Bi $(NO_3)_3{\cdot}5H_2O$, $Na_2WO_4{\cdot}2H_2O$, cetyltrimethylammonium bromide (CTAB) and rhodamine B (RhB) were obtained for use as the raw materials. Graphene oxide (GO) was purchased from Tanfeng Technology Co., Ltd.

2.2 Preparation of Bi_2WO_6/GO deposited PET fabric

Firstly, PET fabric was cut into the size of 5 cm × 5 cm and then was put into the mixed solution containing ethanol and acetone with volume ratio of 1:1, cleaned under ultrasonic stirring at 50 °C for 30 min and dried. 0.2 g as-prepared Bi_2WO_6/GO was dispersed in 50 mL deionized water (DI). Subsequently, PET fabric was dipped into Bi_2WO_6/GO suspension and shaked in the shaker (SHA-C, Jintan Kexi Instrument Co., Ltd.) for 2 h. The obtained Bi_2WO_6/GO deposited PET fabric samples were rinsed in DI water several times and dried. Additionally, 0.2 g Bi_2WO_6 powder was also deposited on the PET fabric according to the similar procedure for comparison.

In detail, Bi_2WO_6/GO composites were prepared by a hydrothermal process. 15 mL GO solution (0.5 g/L, 1 g/L, 2 g/L, 3 g/L and 4 g/L) were added into deionized water, being sonicated for 1 h to produce a homogeneous solution. 0.3 g $Na_2WO_4{\cdot}2H_2O$ and 0.1 g CTAB were then added into the GO solution. The mixture was then stirred and sonicated for 30 min. After that, 0.8 g Bi $(NO_3)_3{\cdot}5H_2O$ was placed into the above mixture solution. Subsequently, the suspension was placed into a 50 mL Teflon-lined autoclave and heated at 120 °C for 8 h. Finally, the product was rinsed in DI and ethanol, and dried at 65 °C. Meanwhile, Bi_2WO_6 photocatalyst was also synthesized without GO.

2.3 Characterizations

Chemical composition of Bi_2WO_6 and Bi_2WO_6/2 g/L GO deposited PET fabrics were conducted by X-ray photoelectron spectroscopy (XPS) spectra with a spectrometer (Kratos XSAM800) using an Al Kα X-ray source (1486.6 eV photons). Raman spectra of Bi_2WO_6, GO and Bi_2WO_6/2 g/L GO powders were performed by a Raman spectrometer (LabRAM HR, France). Surface morphologies of Bi_2WO_6/GO deposited PET fabric and Bi_2WO_6/GO composite were obtained through SEM (JEOL JSM-6700F) and TEM (Tecnai G2 F20 S-TWIN), respectively. The XRD patterns of the products were analyzed using X' Pert PRO diffractometer with Cu Kα radiation (λ = 1.54056 Å) in the 2θ ranging from 10° to 80°. UV-vis spectra were used to characterize the optical property of all the samples and the spectra of the Bi_2WO_6/GO deposited PET fabrics were examined by UV-vis spectrophotometer (UV-2700) from 200 to 800 nm. PL spectra of Bi_2WO_6 and Bi_2WO_6/GO deposited PET fabrics were recorded using a F-7000 fluorescence spectrophotometer. The surface areas of Bi_2WO_6/GO composite were investigated by BET equipment (Gemini VII 2390).

2.4 Photocatalytic activity evaluation

The photocatalytic properties were studied by degradation of RhB. A 500 W xenon lamp (GXZ500, Shanghai, China) with a 420 nm UV-cut filter was utilized as the visible light source. The typical experiment processes were referred to our previous studies [20]. All the samples were immersed in 10 mg/L of RhB (50 mL) aqueous solution. Absorbance of RhB was recorded by a UV-vis spectrophotometer (554 nm for RhB). Absorbance ratio

(A_t/A_0) of RhB was used to evaluate photocatalytic degradation properties of Bi_2WO_6/GO deposited PET fabrics. According to the A_t and A_0, removal rate of RhB (R_{RhB}) and k value were calculated according to the Eqs. (1) and (2) [22, 23]:

$$R_{RhB} = (A_0 - A_t)/A_0 \times 100\% \quad (1)$$

$$-\ln\frac{At}{A0} = kt \quad (2)$$

where A_0 and A_t are the initial absorbance of RhB; the absorbance of RhB at certain reaction time t (min), respectively; k and t are the rate constant and the total irradiation time, respectively.

For the purpose of comparison, photoactivity decomposition of RhB with Bi_2WO_6 deposited PET fabric was also evaluated under the similar conditions. Additionally, influences of deposit weight of Bi_2WO_6/2 g/L GO and initial concentration of dye on the removal rate of RhB were studied. In order to understand the main reactive species, ethylenediaminetetraacetic acid disodium salt (EDTA-2Na), benzoquinone (BQ) and isopropanol (IPA) were used as the scavengers of photoexcited holes (h^+), superoxide radical ($\cdot O_2^-$) and hydroxyl radical (·OH), respectively.

3 Results and discussion

3.1 XPS and Raman spectra

Chemical compositions of Bi_2WO_6 and Bi_2WO_6/GO deposited PET fabrics were studied by XPS spectroscopy (Fig. 1a-e). It can be seen that the two samples mainly contain Bi, W, O and C elements as shown in Fig. 1a. High resolution W 4f XPS spectrum of the sample is presented in Fig. 1b. The peaks with binding energy at 34.8 eV and 36.9 eV correspond to W $4f_{7/2}$ and W $4f_{5/2}$, respectively, which is attributed to a W^{6+} oxidation state

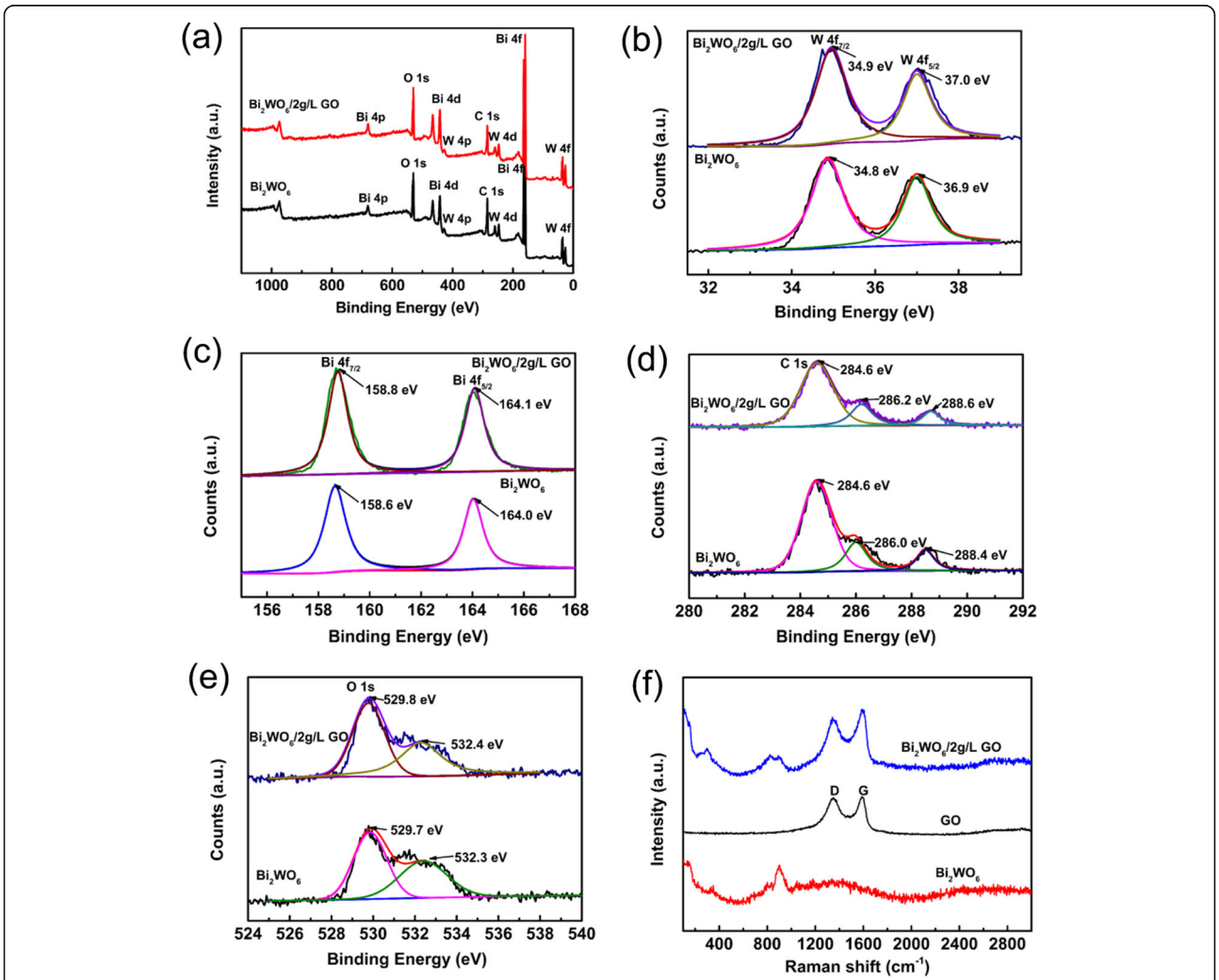

Fig. 1 (**a**) XPS spectra and (**b**) W 4f, (**c**) Bi 4f, (**d**) C 1 s and (**e**) O 1 s of Bi_2WO_6 and Bi_2WO_6/GO deposited PET fabrics; (**f**) Raman spectra of Bi_2WO_6, GO and Bi_2WO_6/GO composite

[24]. The binding energies at 158.6 eV and 164.0 eV are attributed to Bi $4f_{7/2}$ and Bi $4f_{5/2}$ (Fig. 1c), respectively. The result shows that Bi^{3+} exists in Bi_2WO_6 deposited PET fabric [25]. However, the peaks of W 4f and Bi 4f in the Bi_2WO_6/GO deposited PET fabric shift toward high binding energy, which suggests interaction between Bi_2WO_6 and GO [26, 27]. The C 1 s XPS spectrum of the Bi_2WO_6 deposited PET fabric in Fig. 1d is deconvolved into three peaks due to C-C (284.6 eV), C-O (286.0 eV) and C=O (288.4 eV) in epoxy or hydroxyl forms, and the similar peaks are observed in the Bi_2WO_6/GO deposited PET fabric, indicating that GO exists in the composite. Compared with the Bi_2WO_6 deposited PET fabric, the O 1 s spectrum of the Bi_2WO_6/GO deposited PET fabric also exhibits the higher binding energy (Fig. 1e). All these results indicate the interface interaction between GO and Bi_2WO_6, affecting the electronic structure of Bi_2WO_6. In order to further study the structure of Bi_2WO_6/GO composite, Raman was used and the result is shown in Fig. 1f. It can be found that the peaks at 800 and 826 cm^{-1} are attributed to symmetric and antisymmetric modes of terminal O-W-O due to the presence of Bi_2WO_6 [28]. The peak at about 400 cm^{-1} is ascribed to the simultaneous motions of Bi^{3+} and WO_6^{6-}. In the case of GO, the positions of 1334 cm^{-1} and 1594 cm^{-1} displays the characteristic peaks of D-band and G-band, which corresponds to the vibrational mode of E_{2g} phonons of two dimensional sp^2 hybridized carbon network in a six edged lattice with breathing mode of j-joint photons of A_{1g} symmetry [29]. Similarly, for the spectrum of Bi_2WO_6/GO composite, the characteristic peaks of GO and Bi_2WO_6 can be observed, indicating that the Bi_2WO_6/GO composite is successfully synthesized.

3.2 Morphology

SEM and TEM were used to study surface morphology of Bi_2WO_6 and Bi_2WO_6/GO deposited PET fibers and detailed structure of the Bi_2WO_6/GO composite. The surfaces of the fibers become rough after deposition of Bi_2WO_6 (Fig. 2a). Bi_2WO_6 are aggregated together to form larger particles. Figure 2b shows that Bi_2WO_6/GO are deposited on the PET fibers densely and the morphology of the Bi_2WO_6/GO deposited PET fibers is similar to that of Bi_2WO_6 deposited PET fibers. This indicates that the introduction of GO has no obvious effect on the Bi_2WO_6 structure [30]. The structure of Bi_2WO_6/GO composite photocatalyst was observed under transmission electron microscope as shown in Fig. 2c and d. Therefore, Bi_2WO_6 are randomly located on the surfaces or edges of GO, indicating the formation of Bi_2WO_6/GO.

3.3 Crystal structure

XRD patterns of Bi_2WO_6 and Bi_2WO_6/GO deposited PET fabrics were presented in Fig. 3. Figure 3a shows the crystal structures of the pristine Bi_2WO_6 and

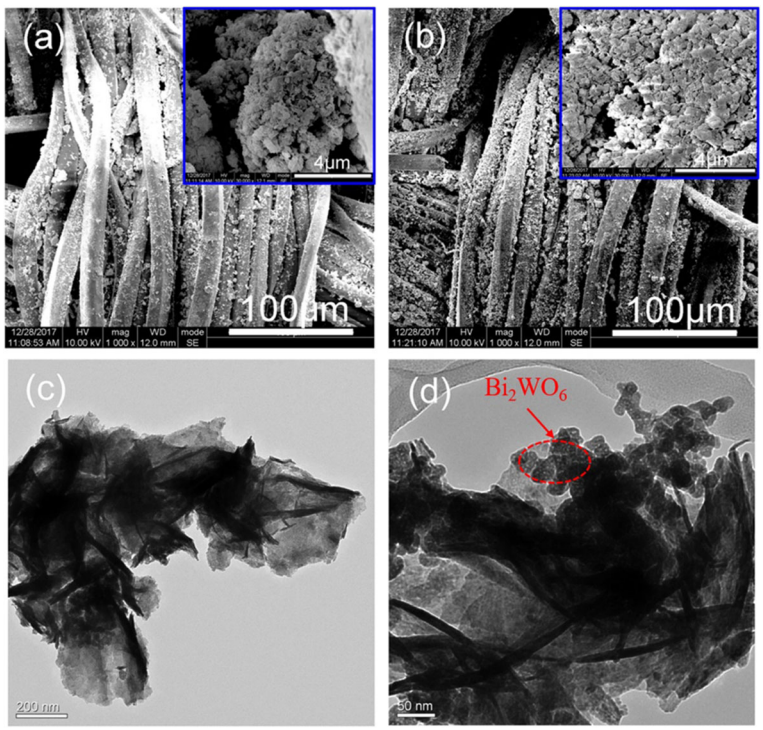

Fig. 2 SEM image of Bi_2WO_6 (**a**) and Bi_2WO_6/GO deposited PET fibers (**b**); TEM images of the Bi_2WO_6/GO composites (**c**, **d**)

Bi_2WO_6/GO particles. The diffraction peaks of pristine Bi_2WO_6 at 2θ of 28.6°, 32.9°, 47.3°, 56.1° and 68.7° are observed. All the diffraction peaks are consistent with the Bi_2WO_6 of the orthogonal crystal phase (JCPDS no. 39–0256). From Fig. S1, GO exhibits a strong peak at 2θ = 10.36° which is ascribed to the (002) plane [31]. In addition, compared with pristine Bi_2WO_6 particles, the diffraction peaks of Bi_2WO_6/GO don't change significantly. This result indicates that the crystal structure of Bi_2WO_6 is not damaged after the introduction of GO because of the small amount of GO in the Bi_2WO_6/GO composite. Figure 3b illustrates the XRD patterns of the Bi_2WO_6 and Bi_2WO_6/GO deposited PET fabrics. The diffraction peaks of Bi_2WO_6 can be observed on the PET fabric, and the peaks at 17.7°, 22.8° and 25.7° are attributed to the characteristic peaks of the pristine PET fabric in all the samples as show in Fig. S1 [32]. This result shows that the Bi_2WO_6/GO composite photocatalysts are deposited on PET fabric.

3.4 UV-vis DRS

UV-vis DRS of as-prepared Bi_2WO_6/GO deposited PET fabrics were investigated as presented in Fig. 4a. Bi_2WO_6/GO deposited PET fabrics have a wider absorption than pristine Bi_2WO_6 deposited PET fabric. In addition, when the content of GO is lower than 2 g/L, the absorption intensity of Bi_2WO_6/GO deposited PET fabrics increases as the content of GO rises. However, the absorption of the deposited fabric does not move to long wavelengths when GO continues to increase, which is in consistent with previous reports [33, 34]. The band gaps are estimated from the $(\alpha h\upsilon)^2$ versus photon energy (hυ) plots and the results are 2.69 eV (Bi_2WO_6/2 g/L GO deposited PET fabric) and 2.81 eV (Bi_2WO_6 deposited PET fabric), respectively, as shown in Fig. 4b. The phenomenon can be explained by the fact that the introduction of GO can effectively narrow down the band gap, thus electron-hole pairs of the sample can separate more easily, further the transfers of photogenerated carriers can be promoted.

In order to determine the positions of the valence band (VB) and conduction band (CB) edges, the ultraviolet-visible diffuse reflectance spectra (DRS), Mott-Schottky plot and valence band X-ray photoelectron spectroscopy (VB XPS) of Bi_2WO_6/2 g/L GO composite were performed and the results are shown in Fig. 4c-e. The results show that the Fermi energy level (E_f), the energy gap between the valence band and the Fermi level (E_{vf}) and the band gap for Bi_2WO_6/2 g/L GO composite are 0.01 eV (vs NHE), 1.90 eV and 2.69 eV, respectively. Therefore, combining with the results of DRS, Mott-Schottky plot and VB XPS, VB and CB edges can be calculated to be 1.91 eV and − 0.78 eV for the Bi_2WO_6/2 g/L GO composite, respectively.

3.5 Surface area

The surface areas of Bi_2WO_6 and Bi_2WO_6/GO composite photocatalyst particles are presented in Fig. 5. It is found that the specific surface areas of pure Bi_2WO_6 and Bi_2WO_6/GO particles are 51.52, 46.15, 47.15, 54.06, 48.82 and 42.44 m^2/g, respectively. This result shows that the surface area of Bi_2WO_6 rises and then reduces with an increase of content of GO, which contributes to adsorb more active substances and further could enhance the photocatalytic properties [35].

3.6 PL analysis

The charge transfer and separation behaviors of the Bi_2WO_6 and Bi_2WO_6/2 g/L GO samples were investigated and the PL spectra of Bi_2WO_6 and Bi_2WO_6/2 g/L GO deposited PET fabric are shown in Fig. 6. It can be found that the two samples have strong emission peaks

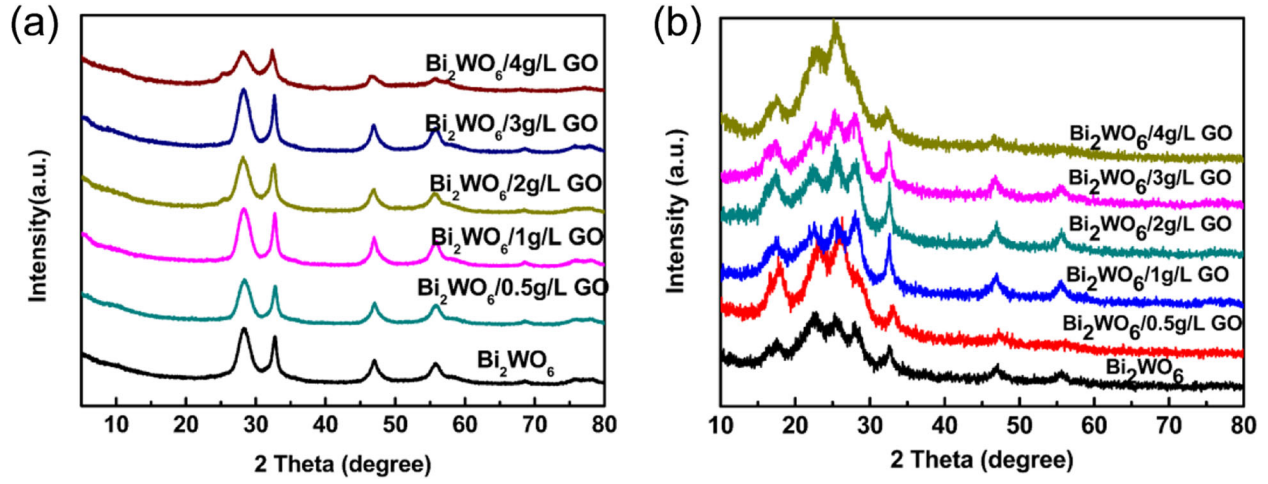

Fig. 3 XRD patterns of (**a**) Bi_2WO_6 and Bi_2WO_6/GO particles, (**b**) Bi_2WO_6 and Bi_2WO_6/GO deposited PET fabrics with different concentrations of GO

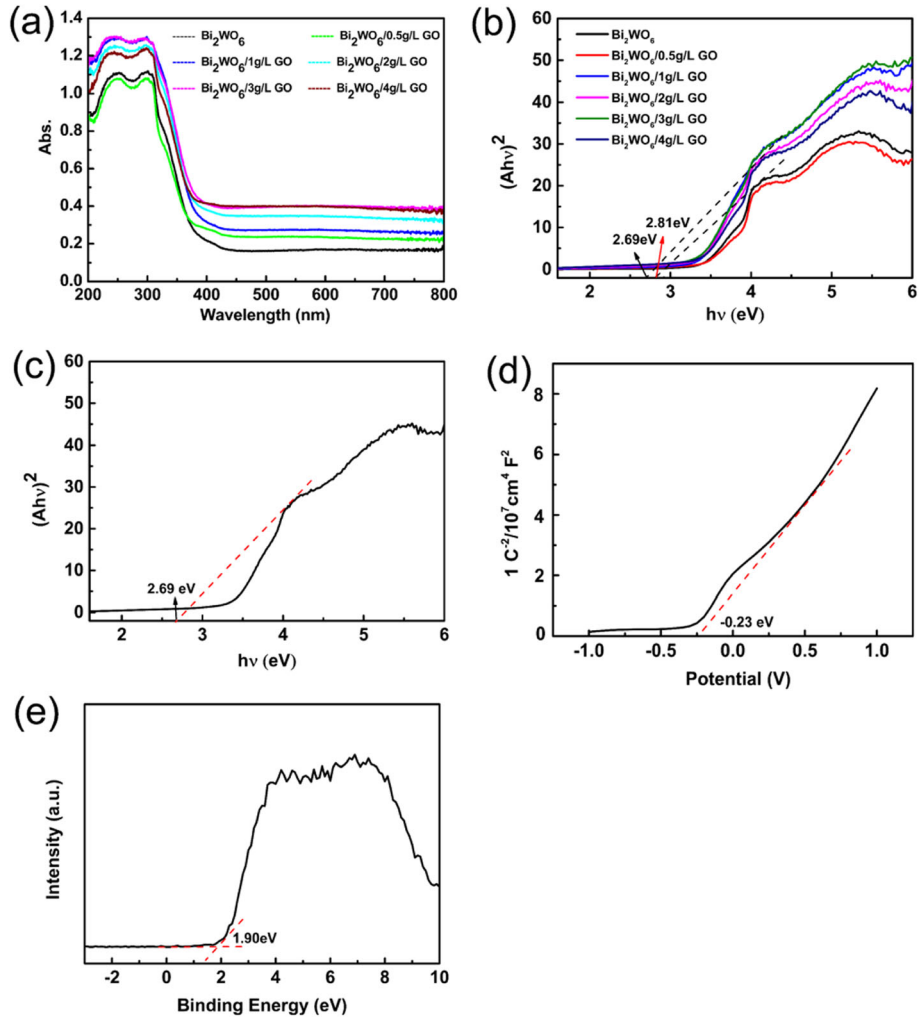

Fig. 4 (**a**) UV-vis DRS and (**b**) Band gaps of all the Bi_2WO_6 and Bi_2WO_6/GO deposited PET fabrics; (**c**) Band gap; (**d**) Mott-Schottky plot vs. saturated calomel electrode (SCE) and (**e**) VB XPS spectrum of Bi_2WO_6/2 g/L GO composite

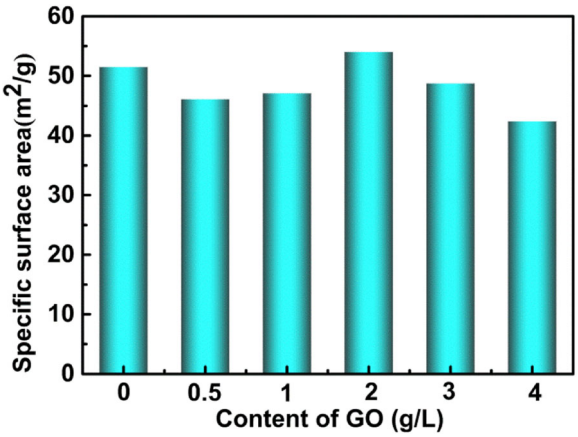

Fig. 5 The BET specific surface areas of Bi_2WO_6 and Bi_2WO_6/GO particles

at 455 nm. However, the intensity of Bi_2WO_6/2 g/L GO deposited PET fabric is lower than that of Bi_2WO_6 deposited PET fabric, indicating that Bi_2WO_6/2 g/L GO deposited PET fabric exhibits a high separation rate of photoinduced electron-hole pairs. Thus, introduction of GO can inhibit recombination of photo-generated carriers of Bi_2WO_6 and improve the photocatalytic properties, which is in good agreement with other reports [36].

3.7 Photocatalytic properties of Bi_2WO_6/GO deposited PET fabrics

Before carrying out the photocatalytic experiment, the adsorption properties of different samples in the dark were explored first and the result is shown in Fig. 7a. It can be seen that all the samples exhibit good adsorption property for RhB. The adsorption of RhB by the samples has reached saturation for 120 min. Especially, the adsorption efficiency of RhB over Bi_2WO_6/GO deposited

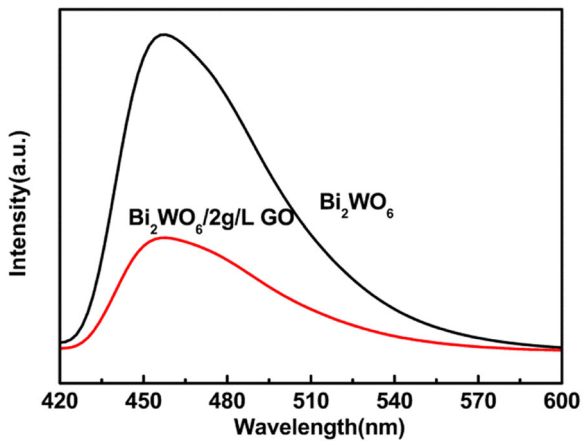

Fig. 6 PL spectra of the Bi_2WO_6 and Bi_2WO_6/2 g/L GO deposited PET fabric (excitation wavelength:405 nm)

PET fabric reaches the highest when the concentration of GO is 2 g/L due to strong hydrophilic properties of GO. The photocatalytic degradation for RhB over Bi_2WO_6/GO deposited PET fabrics was then tested under visible light and the results are shown in Fig. 7b and c. The RhB degradation rates for Bi_2WO_6 and Bi_2WO_6/GO deposited PET fabrics with different concentrations of GO are 82.1%, 88.5%, 89.5%, 94.8%, 92.3% and 90.6%, respectively, when subjected to visible light irradiation for 120 min. Compared with the Bi_2WO_6 deposited PET fabric, the Bi_2WO_6/GO deposited PET fabrics exhibit improved photodegradation performance. In addition, it can be observed that the photocatalytic efficiency of the Bi_2WO_6/GO deposited PET fabric increases gradually and then decreases when the concentration of GO increases. And the Bi_2WO_6/GO deposited PET fabric exhibits the best photocatalytic property when the concentration of GO reaches 2 g/L because the increase of GO content can widen the absorption of visible light, thus resulting in the enhancement of photocatalytic properties. However, degradation rate of RhB on Bi_2WO_6/GO deposited PET fabric decreases when the concentration of GO further rises due to limitation of visible light absorption of Bi_2WO_6. Meanwhile, the photodegradation process fits with the pseudo-first-order kinetics and the maximum rate constant k (Bi_2WO_6/2 g/LGO deposited PET fabric: 0.024 min^{-1}) is 1.7 times than Bi_2WO_6 deposited PET fabric (0.014 min^{-1}).

The UV-vis spectra of RhB over Bi_2WO_6/2 g/LGO deposited PET fabric during the photodegradation process were measured and the result is presented in Fig. 7d. It can be seen that the characteristic peak of RhB is 554 nm and a rapid decline of RhB adsorption is detected, while the spectral maximum shifts from 554 to 496 nm. This is because the release of N-ethyl groups and elimination of the conjugated structure from RhB during photodegradation make the spectrum shift to shorter wavelength [37]. The result demonstrates that RhB is degraded to CO_2, H_2O and other small molecules.

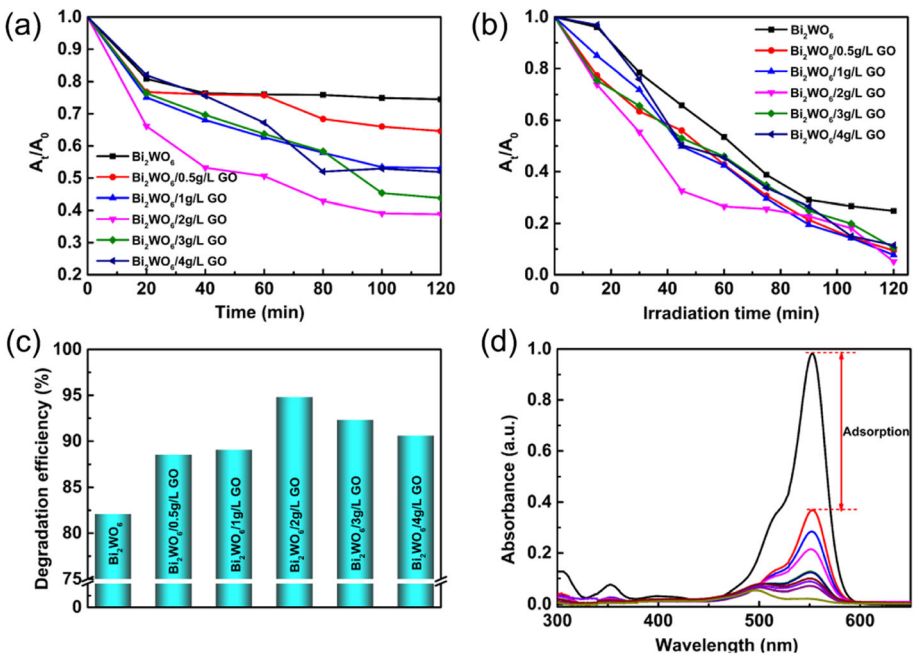

Fig. 7 (**a**) Adsorption of RhB over different samples in the dark; (**b**) Absorbance of different samples for RhB under visible light irradiation; (**c**) Degradation efficiency of RhB over different samples and (**d**) UV-Vis absorption spectra of RhB by Bi_2WO_6/2 g/L GO deposited PET fabric

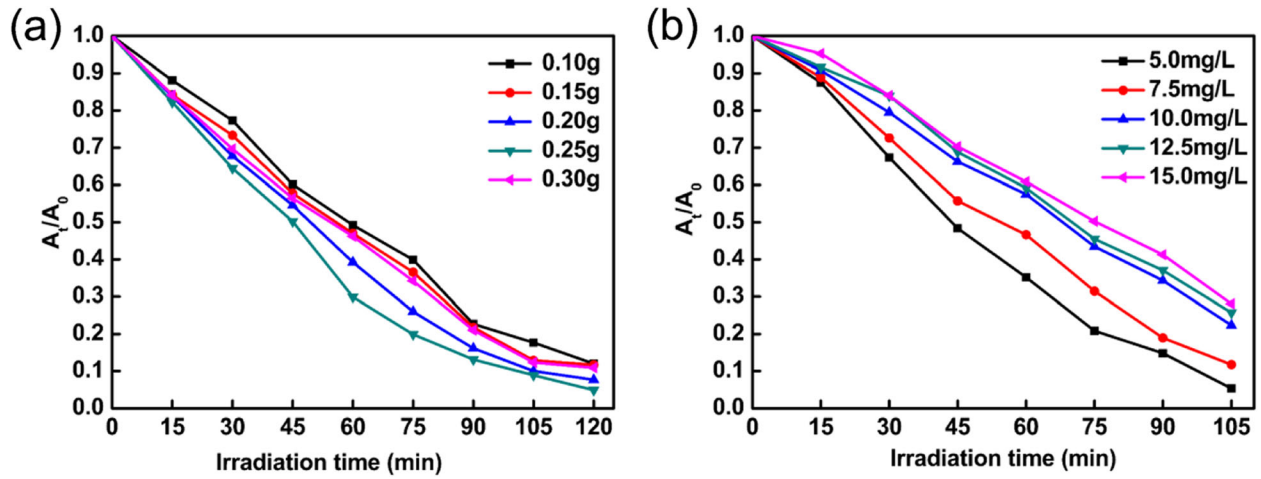

Fig. 8 Effect of (**a**) Bi_2WO_6/2 g/L GO dosage and (**b**) initial concentration of the dye on the removal rate of RhB by Bi_2WO_6/2 g/L GO deposited PET fabric

3.8 Effects of Bi_2WO_6/2 g/L GO content and concentration of RhB on photocatalytic performance

The effect of Bi_2WO_6/2 g/L GO dosage and concentration of the dye solution on removal rate of RhB in the presence of the deposited PET fabric is shown in Fig. 8a and b. The removal rate of RhB rises from 86.8% to 97.3% when the amount of Bi_2WO_6/2 g/LGO photocatalyst on the fabric increases from 0.10 g to 0.25 g as shown in Fig. 8a. However, the removal rate of RhB decreases when the dosage of Bi_2WO_6/2 g/L GO photocatalyst is further increased. This phenomenon may be explained by that the rise of amount of Bi_2WO_6/2 g/L GO will increase the reaction sites that can generate more reactive oxidants. However, the overweight of photocatalysts would increase light scattering and reduce the transmittance, resulting in a decrease in the degradation efficiency of contaminants [20]. From Fig. 8b, the obtained catalysis rates of the samples are 0.028, 0.020, 0.014, 0.013 and 0.011 min^{-1}, respectively, according to the Formula (2). It can be included that the catalysis rate reduces when the concentration of RhB rises because low concentration of dye increases the path length of the photons which enters the solution of dyes, and finally increase amount of photon absorption of photocatalyst [38].

3.9 Recycle stability and trapping experiment of Bi_2WO_6/2 g/L GO deposited PET fabric

The photocatalytic recycle stability of Bi_2WO_6/2 g/L GO deposited PET fabric under visible light is presented in Fig. 9a. Removal rate of RhB in the presence of Bi_2WO_6/2 g/L GO deposited PET fabric is 95% after the first cycle. The removal rate of RhB is 89% after the third cycle. The results show that the photodegradation efficiency of Bi_2WO_6/2 g/L GO deposited PET fabric slightly reduces

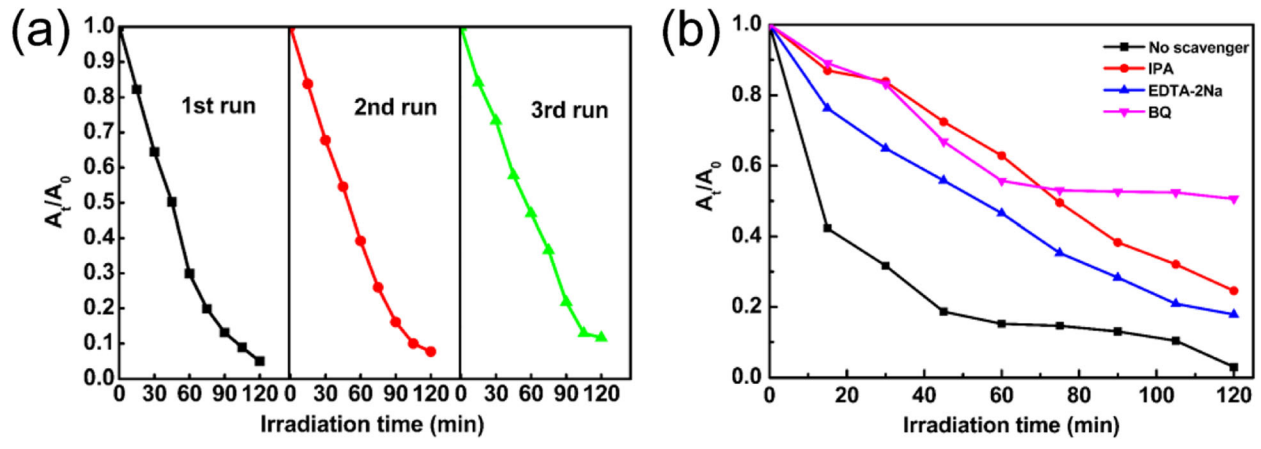

Fig. 9 (**a**) Photodegradation cycles stability of RhB (10 mg/L; 50 mL) by Bi_2WO_6/2 g/L GO deposited PET fabric; (**b**) Trapping experiment of active species during the degradation of RhB by Bi_2WO_6/2 g/L GO deposited PET fabric under visible light irradiation

after three times recycle under visible light irradiation. This is because the photocatalyst deposited on the fabric will be lost to a certain extent during its repeated use. Meanwhile, the surface of the photocatalyst on the fabric will absorb the by-product after the reaction, making the active site reduce. However, the stability of Bi_2WO_6/2 g/L GO deposited PET fabric is good. In order to study the main active species during the photocatalytic process, the trapping experiment was carried out and EDTA-2Na, BQ and IPA were used as h^+, $\cdot O_2^-$ and ·OH scavenger, respectively. Figure 9b shows the effect of different scavengers on the degradation of RhB over Bi_2WO_6/2 g/L GO deposited PET fabric. The result shows that the degradation rate of RhB declines significantly in the presence of BQ. However, the addition of IPA and EDTA-2Na has only a weak inhibitory effect on the degradation of RhB. Therefore, the result demonstrates that $\cdot O_2^-$ plays dominant role in the photodegradation of RhB.

4 Conclusions

In conclusion, Bi_2WO_6/GO composite photocatalysts were successfully fabricated via a simple hydrothermal process and they were then deposited on the PET fabric. Compared with the Bi_2WO_6 deposited PET fabric, the Bi_2WO_6/GO deposited PET fabrics show enhanced photocatalytic activity for RhB. The removal rate of RhB with Bi_2WO_6/GO deposited PET fabric is highest when the content of GO reaches to 2 g/L. Additionally, Bi_2WO_6/2 g/L GO deposited PET fabric shows excellent cycle stability for RhB degradation. This study provides insights into the preparation of modified photocatalysts deposited textiles for organic wastewater treatment.

5 Supplementary information

Supplementary information accompanies this paper at https://doi.org/10.1186/s42825-020-00029-w.

Additional file 1: Fig. S1. XRD patterns of (a) GO and (b) pure PET fabric.

Acknowledgements

This work was financially supported by Joint Fund of the National Natural Science Foundation of China (No. U1833118) and Sichuan Science and Technology Program (2019YFG0244).

Authors' contributions

All authors read and approved the final manuscript.

Authors' information

Not applicable.

Funding

Joint Fund of the National Natural Science Foundation of China (No. U1833118) and Sichuan Science and Technology Program (2019YFG0244).

Availability of data and materials

Not applicable.

Competing interests

The authors declare that they have no competing interests.

Author details

[1]State Key Laboratory of Polymer Materials Engineering of China (Sichuan University), Polymer Research Institute of Sichuan University, Chengdu 610065, China. [2]College of Biomass Science and Engineering, Sichuan University, No.24 South Section 1, Yihuan Road, Chengdu, China. [3]Institute of Textiles and Clothing, The Hong Kong Polytechnic University, Hung Hom, Kowloon, Hong Kong, China.

Received: 14 October 2019 Accepted: 21 June 2020
Published online: 09 October 2020

References

1. Vaiano V, Iervolino G. Facile method to immobilize ZnO particles on glass spheres for the photocatalytic treatment of tannery wastewater. J Colloid Interf Sci. 2018;518:192–9.
2. Zhang M, Lin KYA, Huang C, Tong S. Enhanced degradation of toxic azo dye, amaranth, in water using Oxone catalyzed by MIL-101-NH_2 under visible light irradiation. Sep Purif Technol. 2019;227:115632–40.
3. Beltrán F, Álvarez P, Gimeno O. Graphene-based catalysts for ozone processes to decontaminate water. Molecules. 2019;24:3438–68.
4. Meng X, Zhang Z. Bi_2MoO_6 co-modified by reduced graphene oxide and palladium (Pd^{2+} and Pd^0) with enhanced photocatalytic decomposition of phenol. Appl Catal B Environ. 2017;209:383–93.
5. He R, Cao S, Zhou P, Yu J. Recent advances in visible light bi-based photocatalysts. Chinese J Catal. 2014;35:989–1007.
6. Meng X, Zhang Z. Bismuth-based photocatalytic semiconductors: introduction, challenges and possible approaches. J Mol Catal A Chem. 2016;423:533–49.
7. Meng X, Li Z, Zhang Z. Palladium nanoparticles and rGO co-modified $BiVO_4$ with greatly improved visible light-induced photocatalytic activity. Chemosphere. 2018;198:1–12.
8. Fan Z, Shi H, Zhao H, Cai J, Zhao G. Application of carbon aerogel electrosorption for enhanced Bi_2WO_6 photoelectrocatalysis and elimination of trace nonylphenol. Carbon. 2018;126:279–88.
9. Phuruangrat A, Maneechote A, Dumrongrojthanath P, Ekthammathat N, Thongtem S, Thongtem T. Effect of pH on visible-light-driven Bi_2WO_6 nanostructured catalyst synthesized by hydrothermal method. Superlattice Microst. 2015;78:106–15.
10. Ju P, Wang Y, Sun Y, Zhang D. Controllable one-pot synthesis of a nest-like Bi_2WO_6/$BiVO_4$ composite with enhanced photocatalytic antifouling performance under visible light irradiation. Dalton Trans. 2016;45:4588–602.
11. Liu Y, Chen L, Yuan Q, He J, Au C, Yin S. A green and efficient photocatalytic route for the highly-selective oxidation of saturated alpha-carbon C-H bonds in aromatic alkanes over flower-like Bi_2WO_6. Chem Commun. 2016;52:1274–7.
12. Chen C, Cao S, Yu W, Xie X, Liu Q, Tsang Y, Xiao Y. Adsorption, photocatalytic and sunlight-driven antibacterial activity of Bi_2WO_6/graphene oxide nanoflakes. Vacuum. 2015;116:48–53.
13. Meng X, Zhang Z. Ag/AgCl loaded Bi_2WO_6 composite: a plasmonic Z-scheme visible light-responsive photocatalyst. Int J Photoenergy. 2016. https://doi.org/10.1155/2016/4054351.
14. Dumrongrojthanath P, Thongtem T, Phuruangrat A, Thongtem S. Synthesis and characterization of hierarchical multilayered flower-like assemblies of Ag doped Bi_2WO_6 and their photocatalytic activities. Superlattice Microst. 2013;64:196–203.
15. Zeng Q, Xie X, Wang X, Lu G, Li H, Lee S, Sun J. New insights into the synergistic effect of active radicals and adsorptive ability on the photodegradation of gaseous acetaldehyde over reduced graphene oxide/P25 composite. J Hazard Mater. 2019;380:12081–9.
16. Lv N, Li Y, Huang Z, Li T, Ye S, Dionysiou D, Song X. Synthesis of GO/TiO_2/Bi_2WO_6 nanocomposites with enhanced visible light photocatalytic degradation of ethylene. Appl Catal B Environ. 2019;246:303–11.
17. Qian Y, Feng J, Fan D, Zhang Y, Kuang X, Wang H, Wei Q, Ju H. A sandwich-type photoelectrochemical immunosensor for NT-pro BNP detection based on F-Bi_2WO_6/Ag_2S and GO/PDA for signal amplification. Biosens Bioelectron. 2019;131:299–306.
18. Zhai J, Yu H, Li H, Sun L, Zhang K, Yang H. Visible-light photocatalytic activity of graphene oxide-wrapped Bi_2WO_6 hierarchical microspheres. Appl Surf Sci. 2015;344:101–6.

19. Li Y, Chen L, Wang Y, Zhu L. Advanced nanostructured photocatalysts based on reduced grapheme oxide-flower-like Bi_2WO_6 composites for an augmented simulated solar photoactivity activity. Mat Sci Eng B. 2016;210:29–36.
20. Du Z, Cheng C, Tan L, Lan J, Jiang S, Zhao L, Guo R. Enhanced photocatalytic activity of Bi_2WO_6/TiO_2 composite coated polyester fabric under visible light irradiation. Appl Surf Sci. 2018;435:626–34.
21. Du Z, Guo R, Lan J, Jiang S, Lin S, Cheng C, Zhao L. Bismuth tungstate coating on polyester fabric modified with dopamine for photocatalytic property under visible light irradiation. Surf Coat Tech. 2017;319:219–29.
22. Li C, Chen G, Sun J, Rao J, Han Z, Hu Y, Xing W, Zhang C. Doping effect of phosphate in Bi_2WO_6 and universal improved photocatalytic activity for removing various pollutants in water. Appl Catal B Environ. 2016;188:39–47.
23. Kaur A, Kansal S. Bi_2WO_6 nanocuboids: an efficient visible light active photocatalyst for the degradation of levofloxacin drug in aqueous phase. Chem Eng J. 2016;302:194–203.
24. Jaramillo-Páez C, Navío J, Hidalgo M. Effect of synthesis pH on the physicochemical properties of a synthesized Bi_2WO_6 and the type of substrate chosen, in assessing its photo-catalytic activities. Arab J Chem. 2020;13:431–43.
25. Bunpang K, Wisitsoraat A, Tuantranont A, Phanichphant S, Liewhiran C. Effects of reduced graphene oxide loading on gas-sensing characteristics of flame-made Bi_2WO_6 nanoparticles. Appl Surf Sci. 2019;496:143613.
26. Sun Z, Guo J, Zhu S, Mao L, Ma J, Zhang D. A high-performance Bi_2WO_6-graphene photocatalyst for visible light-induced H_2 and O_2 generation. Nanoscale. 2014;6:2186–93.
27. Tian L, Liu J, Gong C, Ye L, Zan L. Fabrication of reduced graphene oxide-BiOCl hybrid material via a novel benzyl alcohol route and its enhanced photocatalytic activity. J Nanopart Res. 2013;15:1–11.
28. Lei S, Qin C, Tang X, Zhong J, Li J, Chen J. Spiral carbon fibers modified Bi_2WO_6 with enhanced photocatalytic activity. J Phys Chem Solids. 2020;141:109430.
29. Sadhukhan S, Bhattacharyya A, Rana D, Ghosh T, Orasugh J, Khatua S, Acharya K, Chattopadhyay D. Synthesis of RGO/NiO nanocomposites adopting a green approach and its photocatalytic and antibacterial properties. Mater Chem Phys. 2020;247:122906.
30. Wang L, Sun B, Wang W, Feng L, Li Q, Li C. Modification of Bi_2WO_6 composites with rGO for enhanced visible light driven NO removal. Asia Pac J Chem Eng. 2017;12:121–7.
31. Meng X, Zhang Z. Plasmonic ternary Ag-rGO-Bi_2MoO_6 composites with enhanced visible light-driven photocatalytic activity. J Catal. 2016;344:616–30.
32. Sudrajat H, Babel S. A new, cost-effective solar photoactive system N-ZnO@polyester fabric for degradation of recalcitrant compound in a continuous flow reactor. Mater Res Bull. 2016;83:369–78.
33. Ohtsu N, Hiromoto S, Yamane M, Satoh K, Tomozawa M. Chemical and crystallographic characterizations of hydroxyapatite- and octacalcium phosphate-coatings on magnesium synthesized by chemical solution deposition using XPS and XRD. Surf Coat Tech. 2013;218:114–8.
34. Yan Y, Sun S, Song Y, Yan X, Guan W, Liu X, Shi W. Microwave-assisted in situ synthesis of reduced graphene oxide-$BiVO_4$ composite photocatalysts and their enhanced photocatalytic performance for the degradation of ciprofloxacin. J Hazard Mater. 2013;250-251:106–14.
35. Gao M, Zhang D, Li H, Pu X, Shao X, Li W. Enhanced photocatalytic activity of AgCl/BiOCl heterostructures synthesized by a one-pot combustion method. Mater Lett. 2015;159:406–9.
36. Zhao J, Yang Y, Dong X, Ma Q, Yu W, Wang J, Liu G. Electrospinning construction of Bi_2WO_6/RGO composite nanofibers with significantly enhanced photocatalytic water splitting activity. RSC Adv. 2016;6:64741–8.
37. Wang T, Liu S, Mao W, Bai Y, Chiang K, Shah K, Paz-Ferreiro J. Novel Bi_2WO_6 loaded N-biochar composites with enhanced photocatalytic degradation of rhodamine B and Cr (VI). J Hazard Mater. 2020;389:121827.
38. Zhou L, Jin C, Yu Y, Chi F, Ran S, Lv Y. Molten salt synthesis of Bi_2WO_6 powders with enhanced visible-light-induced photocatalytic activities. J Alloy Compd. 2016;680:301–8.

Publisher's Note

Springer Nature remains neutral with regard to jurisdictional claims in published maps and institutional affiliations.

Submit your manuscript to a SpringerOpen journal and benefit from:

- ► Convenient online submission
- ► Rigorous peer review
- ► Open access: articles freely available online
- ► High visibility within the field
- ► Retaining the copyright to your article

Submit your next manuscript at ► springeropen.com